




Crystal structure of flumethasone, C₂₂H₂₈F₂O₅James A. Kaduk^{1,2} , Anja Dosen³  and Thomas N. Blanton³ ¹Department of Chemistry, Illinois Institute of Technology, Chicago, IL, 60616, USA²Department of Physics, North Central College, Naperville, IL, 60540, USA³ICDD, Newtown Square, PA, 19073-3273, USA

(Received 27 November 2024; revised 05 February 2025; accepted 06 February 2025)

Abstract: The crystal structure of flumethasone has been solved and refined using synchrotron X-ray powder diffraction data, and optimized using density functional theory techniques. Flumethasone crystallizes in space group $P2_1$ (#4) with $a = 6.46741(5)$, $b = 24.91607(20)$, $c = 12.23875(11)$ Å, $\beta = 90.9512(6)^\circ$, $V = 1971.91(4)$ Å³, and $Z = 4$ at 298 K. The crystal structure consists of O–H...O hydrogen-bonded double layers of flumethasone molecules parallel to the ac -plane. The powder pattern has been submitted to ICDD for inclusion in the Powder Diffraction File™ (PDF®).

© The Author(s), 2025. Published by Cambridge University Press on behalf of International Center for Diffraction Data. This is an Open Access article, distributed under the terms of the Creative Commons Attribution licence (<http://creativecommons.org/licenses/by/4.0>), which permits unrestricted re-use, distribution and reproduction, provided the original article is properly cited. [doi:10.1017/S0885715625000120]

Key words: flumethasone, flumetasone, crystal structure, Rietveld refinement, density functional theory

I. INTRODUCTION

Flumethasone (also known as flumetasone) is a fluorinated corticosteroid, that has anti-inflammatory, antipruritic, and vasoconstrictive properties. It is administered topically resulting in a reduction in inflammation, exudation, and itching. Flumethasone is approved for human and animal use. The systematic name (CAS Registry Number 2135-17-3) is (6*S*,8*S*,9*R*,10*S*,11*S*,13*S*,14*S*,16*R*,17*R*)-6,9-difluoro-11,17-dihydroxy-17-(2-hydroxyacetyl)-10,13,16-trimethyl-6,7,8,11,12,14,15,16-octahydrocyclopenta[*a*]phenanthren-3-one. A two-dimensional molecular diagram of flumethasone is shown in Figure 1. Although diffraction data for other stereoisomers and related compounds of flumethasone have been published, we are unaware of any X-ray diffraction data on flumethasone itself.

This study was carried out as part of a project (Kaduk et al., 2014) to determine the crystal structures of large-volume commercial pharmaceuticals, and include high-quality powder diffraction data for them in the Powder Diffraction File (Kabekkodu et al., 2024).

II. EXPERIMENTAL

Flumethasone was a commercial reagent, purchased from TargetMol (Batch #T1124), and was used as received. The white powder was packed into a 0.5 mm diameter Kapton capillary and rotated during the measurement at ~2 Hz. The powder pattern was measured at 298(1) K at the Wiggler Low Energy Beamline (Leontowich et al., 2021) of the Brockhouse

X-ray Diffraction and Scattering Sector of the Canadian Light Source using a wavelength of 0.819826(2) Å (15.1 keV) from 1.6 to 75.0° 2 θ with a step size of 0.0025° and a collection time of 3 min. The high-resolution powder diffraction data were collected using eight Dectris Mythen2 X series 1 K linear strip detectors. NIST SRM 660b LaB₆ was used to calibrate the instrument and refine the monochromatic wavelength used in the experiment.

The pattern was indexed using JADE Pro (MDI, 2024) on a primitive monoclinic unit cell with $a = 6.46144$, $b = 24.71548$, $c = 12.15613$ Å, $\beta = 90.67^\circ$, $V = 1941.17$ Å³, and $Z = 4$. The suggested space group was $P2_1$, which was confirmed by the successful solution and refinement of the structure. A reduced cell search of the Cambridge Structural Database (Groom et al., 2016) with the chemistry C, H, F, and O only yielded no hits.

A structural model of the flumethasone molecule was downloaded from PubChem (Kim et al., 2023) as Conformer3D_COMPOUND_CID_16490.sdf. It was converted to a *.mol2 file using Mercury (Macrae et al., 2020). The crystal structure was solved using Monte Carlo simulated annealing techniques as implemented in EXPO2014 (Altomare et al., 2013), using two molecules as fragments and a bump penalty.

Rietveld refinement was carried out with GSAS-II (Toby and Von Dreele, 2013). Only the 3.5–50.0° portion of the pattern was included in the refinements ($d_{\min} = 0.970$ Å). The y -coordinate of F1 was fixed to define the origin. All non-H bond distances and angles were subjected to restraints, based on a Mercury/Mogul Geometry Check (Sykes et al., 2011; Bruno et al., 2004). The Mogul average and standard deviation for each quantity were used as the restraint parameters. The restraints contributed 4.8% to the overall χ^2 . The hydrogen atoms were included in calculated positions, which were

Corresponding author: James A. Kaduk; Email: kaduk@polycrystallography.com



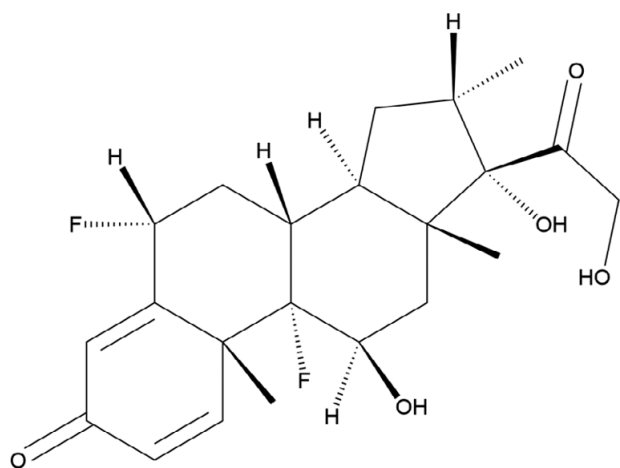


Figure 1. The two-dimensional structure of flumethasone, $C_{22}H_{28}F_2O_5$.

recalculated during the refinement using Materials Studio (Dassault Systèmes, 2023). The U_{iso} of the heavy atoms were grouped by chemical similarity. The U_{iso} for the H atoms was fixed at $1.3 \times$ the U_{iso} of the heavy atoms to which they are attached. The peak profiles were described using the generalized microstrain model (Stephens, 1999). A 2nd-order spherical harmonic model for preferred orientation was included in the refinement. The background was modeled using a 6-term shifted Chebyshev polynomial, with peaks at 10.37° and 40.08° to model the scattering from the Kapton capillary and any amorphous component of the sample.

The final refinement of 207 variables using 18,601 observations and 174 restraints yielded the residual $R_{wp} = 0.05403$. The largest peak (1.69 \AA from C85) and hole (1.16 \AA from C22) in the difference Fourier map were $0.24(6)$ and $-0.24(6) e\text{\AA}^{-3}$, respectively. The final Rietveld plot is shown in Figure 2. The largest features in the normalized error plot are in the shapes of some of the strong low-angle peaks. These

misfits probably indicate subtle changes in the specimen during the measurement.

The crystal structure of flumethasone was optimized (fixed experimental unit cell) with density functional theory techniques using VASP (Kresse and Furthmüller, 1996) through the MedeA graphical interface (Materials Design, 2024). The calculation was carried out on 32 cores of a 144-core (768 Gb memory) HPE Superdome Flex 280 Linux server at North Central College. The calculation used the GGA-PBE functional, a plane wave cutoff energy of 400.0 eV , and a k -point spacing of 0.5 \AA^{-1} leading to a $2 \times 1 \times 2$ mesh, and took $\sim 21 \text{ h}$. Single-point density functional calculations (fixed experimental cell) and population analysis were carried out using CRYSTAL23 (Erba et al., 2023). The basis sets for the H, C, and O atoms in the calculation were those of Gatti et al. (1994), and for F was that of Peintinger et al. (2013). The calculations were run on a 3.5 GHz PC using 8 k -points and the B3LYP functional and took $\sim 7.5 \text{ h}$.

III. RESULTS AND DISCUSSION

There are two molecules in the asymmetric unit of flumethasone. The root-mean-square difference of the non-H atoms in the Rietveld-refined and VASP-optimized structures, calculated using the Mercury CSD-Materials/Search/Crystal Packing Similarity tool, is 0.100 \AA . The root-mean-square Cartesian displacement of the non-H atoms in the Rietveld-refined and VASP-optimized structures of molecules 1 and 2, calculated using the Mercury Calculate/Molecule Overlay tool, are 0.064 and 0.083 \AA (Figures 3 and 4). The agreements are within the normal range for correct structures (van de Streek and Neumann, 2014). The two molecules have similar conformations (Figure 5); the rms displacement is only 0.091 \AA . The asymmetric unit is illustrated in Figure 6. The remaining discussion will emphasize the VASP-optimized structure.

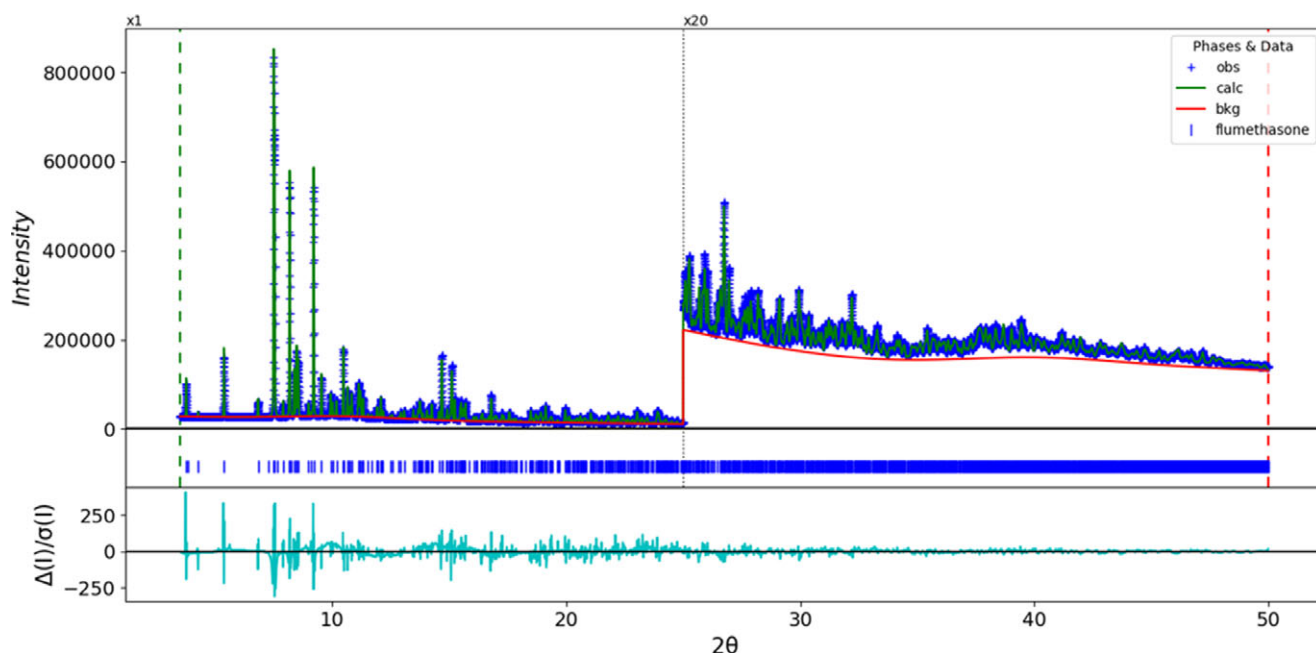


Figure 2. The Rietveld plot for flumethasone. The blue crosses represent the observed data points, and the green line is the calculated pattern. The cyan curve is the normalized error plot, and the red line is the background curve. The vertical scale has been multiplied by a factor of $20 \times$ for $2\theta > 25.0^\circ$.

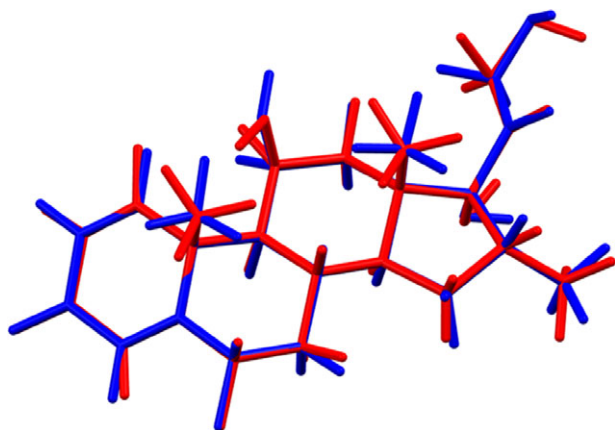


Figure 3. Comparison of the Rietveld-refined (red) and VASP-optimized (blue) structures of molecule 1 of flumethasone. The root-mean-square Cartesian displacement is 0.064 Å. Image generated using Mercury (Macrae et al., 2020).

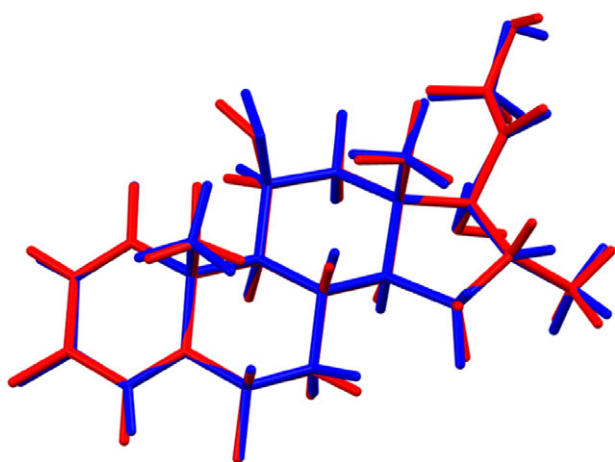


Figure 4. Comparison of the Rietveld-refined (red) and VASP-optimized (blue) structures of molecule 2 of flumethasone. The root-mean-square Cartesian displacement is 0.083 Å. Image generated using Mercury (Macrae et al., 2020).

All bond distances, bond angles, and torsion angles fall within the normal ranges indicated by a Mercury Mogul Geometry check (Macrae et al., 2020). Quantum chemical geometry optimizations of isolated flumethasone molecules (DFT/B3LYP/6-31G*/water) using Spartan '24 (Wavefunction, 2023) indicated that the two molecules converge to the same local minimum (rms difference = 0.012 Å) and are identical in energy. The global minimum-energy conformation (MMFF force field) has the opposite conformation of the side chain but is only 1.7 kcal/mol lower in energy. Intermolecular interactions thus determine the solid-state conformation.

The crystal structure (Figure 7) consists of hydrogen-bonded double layers of flumethasone molecules parallel to the *ac*-plane. The mean planes of the steroid molecules are approximately $-5, 14, 1$ and $5, 13, 1$. Analysis of the contributions to the total crystal energy of the structure using the Forcite module of Materials Studio (Dassault Systèmes, 2023) indicates that the intramolecular energy is dominated by angle distortion terms (as might be expected for a fused ring system), but that bond and torsion distortion terms are also significant. The intermolecular energy is dominated by

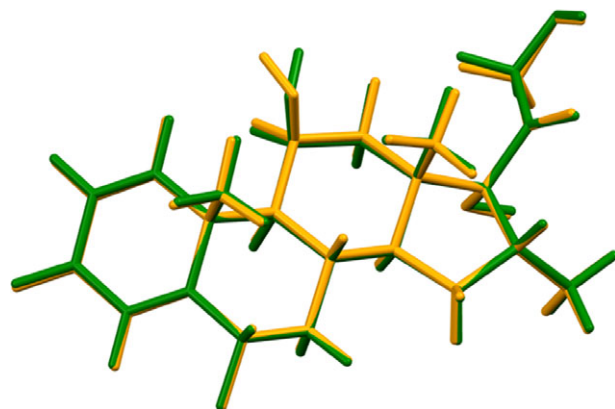


Figure 5. Comparison of molecule 1 (green) and molecule 2 (orange) of flumethasone. The root-mean-square Cartesian displacement is 0.091 Å. Image generated using Mercury (Macrae et al., 2020).

electrostatic repulsions, which in this force field-based analysis also include hydrogen bonds. The hydrogen bonds are better discussed using the results of the DFT calculation.

The hydroxyl groups O6 and O63 in the side chains form O–H...O hydrogen bonds to the carbonyl groups O7 and O64 of adjacent molecules (Table I). In addition, they form intramolecular hydrogen bonds to the carbonyl groups O5 and O62. The O63–H114 hydrogen bond forms a pattern with the graph set (Etter, 1990; Bernstein et al., 1995; Motherwell et al., 2000) $C1, I(14)$, while the O6–H57 hydrogen bond forms a more complicated pattern with graph set $R3, 4(34)$. The hydroxyl groups O4 and O61 act as donors in discrete hydrogen bonds to hydroxyl groups O63 and O6, both with graph set $D1, I(2)$. The hydroxyl groups O3 and O60 form intramolecular hydrogen bonds to the carbonyl groups O7 and O64, both with graph set $C1, I(12)$. The result of these O–H...O hydrogen bonds is a 2-dimensional network parallel to the *ac*-plane. The energies of the O–H...O hydrogen bonds were calculated using the correlation of Rammohan and Kaduk (2018). There are perhaps a surprising number of inter- and intra-molecular C–H...O hydrogen bonds. Molecule 2 acts as a donor in a larger number of these.

The volume enclosed by the Hirshfeld surface of flumethasone (Figure 8; Hirshfeld, 1977; Spackman et al., 2021) is 974.73 \AA^3 , 98.86% of 1/2 of the unit cell volume. The packing density is thus typical. The only significant close contacts (red in Figure 8) involve the hydrogen bonds. The volume/non-hydrogen atom is smaller than normal (Kempster and Lipson, 1972), at 17.0 \AA^3 .

The Bravais–Friedel–Donnay–Harker (Bravais, 1866; Friedel, 1907; Donnay and Harker, 1937) algorithm suggests that we might expect needle morphology for flumethasone, with [100] as the long axis. A 2nd-order spherical harmonic model was included in the refinement. The texture index was 1.021(0), indicating that the preferred orientation was slight in this rotated capillary specimen.

IV. DEPOSITED DATA

The powder pattern of flumethasone from this synchrotron data set has been submitted to ICDD for inclusion in the Powder Diffraction File. The Crystallographic Information Framework (CIF) files containing the results of the Rietveld

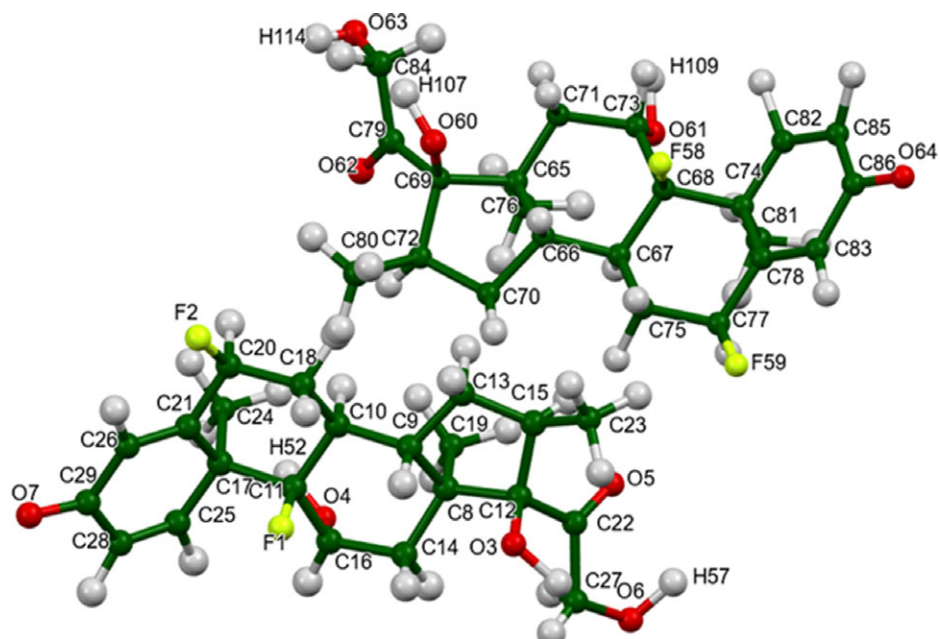


Figure 6. The asymmetric unit of flumethasone, with the atom numbering. The atoms are represented by 50% probability spheroids. Image generated using Mercury (Macrae et al., 2020).

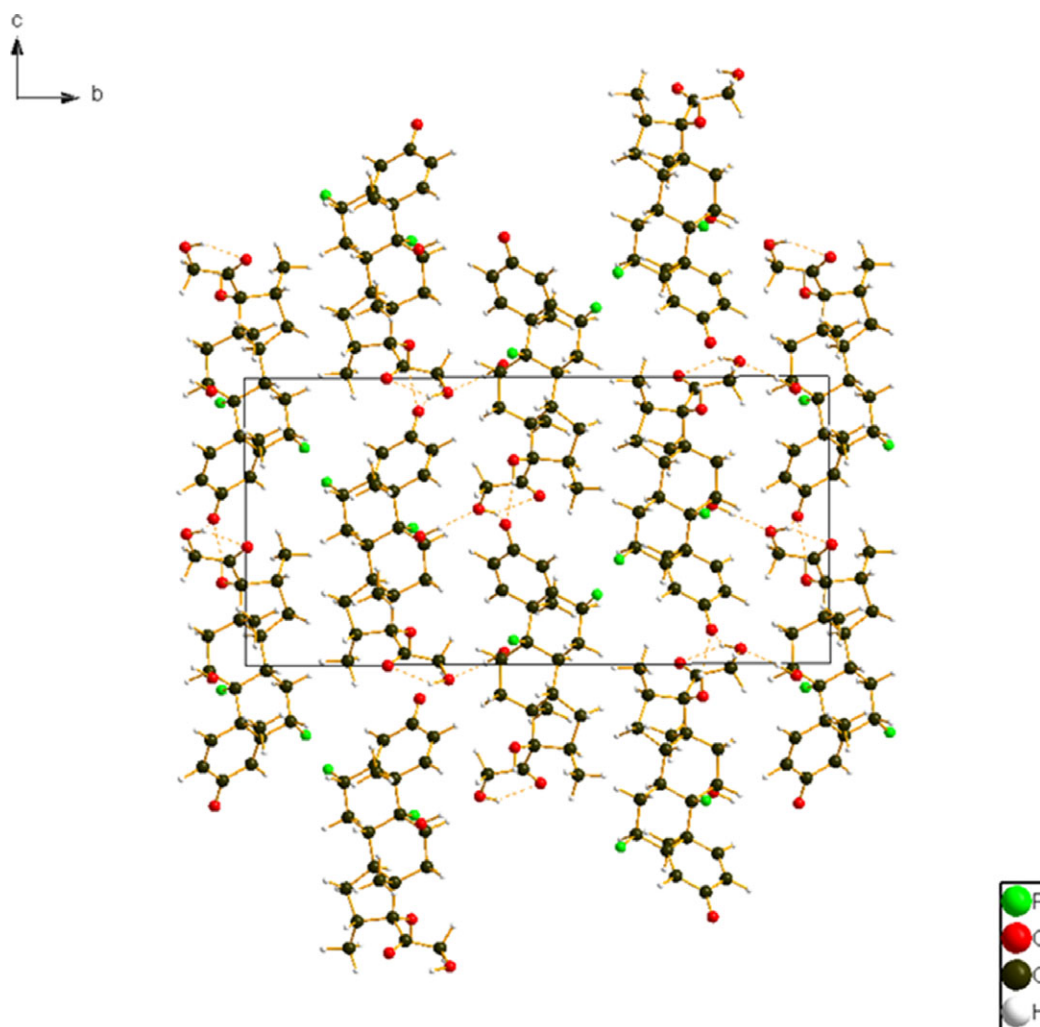


Figure 7. The crystal structure of flumethasone is viewed down the a -axis. Image generated using Diamond (Crystal Impact, 2023).

TABLE I. Hydrogen bonds (CRYSTAL23) in flumethasone.

H-Bond	D–H (Å)	H...A (Å)	D...A (Å)	D–H...A(°)	Mulliken overlap (<i>e</i>)	<i>E</i> (kcal/mol)
O3-H114...O64	0.990	2.102	2.943	141.7	0.027	9.0
O3-H114...O62	0.990	2.119*	2.673	113.5	0.031	9.6
O6-H57...O7	0.990	1.959	2.788	139.7	0.034	10.1
O6-H57...O5	0.990	2.179*	2.681	109.8	0.029	9.3
O61-H109...O6	0.986	1.840	2.813	168.3	0.048	12.0
O4-H52...O63	0.989	1.802	2.778	168.2	0.050	12.2
O60-H107...O64	0.985	2.007	2.953	160.2	0.032	9.8
O3-H50...O7	0.987	1.869	2.837	166.1	0.039	10.8
C85-H113...O3	1.089	2.675	3.496	131.7	0.011	
C84-H111...O64	1.104	2.410	3.372	144.7	0.019	
C27-H55...O7	1.101	2.681	3.501	130.7	0.011	
C82-H108...O6	1.093	2.561	3.649	173.5	0.023	
C25-H51...O4	1.093	2.454*	3.070	114.3	0.019	
C81-H106...O61	1.093	2.274*	2.969	119.6	0.019	
C24-H49...O4	1.094	2.250*	2.943	119.2	0.013	
C80-H101...O62	1.100	2.659	3.731	164.6	0.010	
C73-H94...O7	1.103	2.560	3.613	159.3	0.018	
C72-H93...O62	1.100	2.443*	2.905	103.6	0.010	
C71-H91...O60	1.098	2.428*	2.876	102.7	0.012	
C19-H40...O4	1.095	2.324*	3.012	119.0	0.012	

*intramolecular

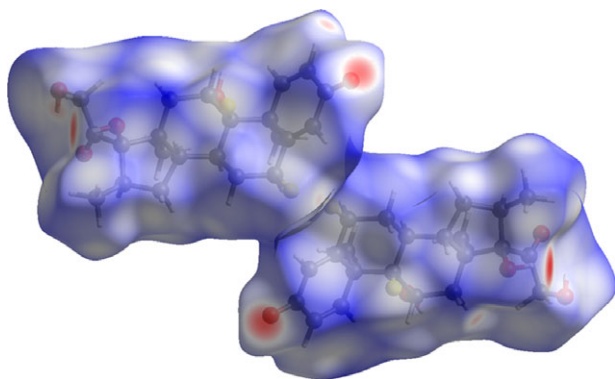


Figure 8. The Hirshfeld surface of flumethasone. Intermolecular contacts longer than the sums of the van der Waals radii are colored blue, and contacts shorter than the sums of the radii are colored red. Contacts equal to the sums of radii are white. Image generated using CrystalExplorer (Spackman et al., 2021).

refinement (including the raw data) and the DFT geometry optimization were deposited with the ICDD. The data can be requested at pdj@icdd.com.

ACKNOWLEDGMENTS

Part or all of the research described in this article was performed at the Canadian Light Source, a national research facility of the University of Saskatchewan, which is supported by the Canada Foundation for Innovation (CFI), the Natural Sciences and Engineering Research Council (NSERC), the Canadian Institute of Health Research (CIHR), the Government of Saskatchewan, and the University of Saskatchewan.

CONFLICTS OF INTEREST

The authors declare no conflicts of interest.

FUNDING STATEMENT

This study was partially supported by the International Centre for Diffraction Data. We thank Adam Leontowich for his assistance in the data collection. We also thank the ICDD team—Megan Rost, Steve Trimble, and Dave Bohnenberger—for their contribution to research, sample preparation, and in-house XRD data collection and verification.

REFERENCES

- Altomare, A., C. Cuocci, C. Giacovazzo, A. Moliterni, R. Rizzi, N. Corriero, and A. Falcicchio. 2013. "EXPO2013: A Kit of Tools for Phasing Crystal Structures from Powder Data." *Journal of Applied Crystallography* 46: 1231–1235.
- Bernstein, J., R. E. Davis, L. Shimoni, and N. L. Chang. 1995. "Patterns in Hydrogen Bonding: Functionality and Graph Set Analysis in Crystals." *Angewandte Chemie International Edition in English* 34: 1555–1573.
- Bravais, A. 1866. *Etudes Cristallographiques*. Paris: Gauthier Villars.
- Bruno, I. J., J. C. Cole, M. Kessler, J. Luo, W. D. S. Motherwell, L. H. Purkis, B. R. Smith, R. Taylor, R. I. Cooper, S. E. Harris, and A. G. Orpen. 2004. "Retrieval of Crystallographically-Derived Molecular Geometry Information." *Journal of Chemical Information and Computer Sciences* 44: 2133–2144.
- Crystal Impact Dr. H. Putz & Dr. K. Brandenburg. 2023. *Diamond V. 5.0.0*. Bonn, Germany.
- Dassault Systèmes. 2023. *BIOVIA Materials Studio 2024*. San Diego, CA: BIOVIA.
- Donnay, J. D. H., and D. Harker. 1937. "A New Law of Crystal Morphology Extending the Law of Bravais." *American Mineralogist* 22: 446–467.
- Erba, A., J. K. Desmarais, S. Casassa, B. Civalieri, L. Donà, I. J. Bush, B. Searle, L. Maschio, L.-E. Daga, A. Cossard, C. Ribaldone, E. Ascrizzi, N. L. Marana, J.-P. Flament, and B. Kirtman. 2023. "CRYSTAL23: A Program for Computational Solid State Physics and Chemistry." *Journal of Chemical Theory and Computation* 19: 6891–6932; <https://doi.org/10.1021/acs.jctc.2c00958>.
- Etter, M. C. 1990. "Encoding and Decoding Hydrogen-Bond Patterns Of Organic Compounds." *Accounts of Chemical Research* 23: 120–126.
- Friedel, G. 1907. "Etudes sur la loi de Bravais." *Bulletin de la Société Française de Minéralogie* 30: 326–455.
- Gatti, C., V. R. Saunders, and C. Roetti. 1994. "Crystal-Field Effects on the Topological Properties of the Electron-Density in Molecular Crystals - the Case of Urea." *Journal of Chemical Physics* 101: 10686–10696.

- Groom, C. R., I. J. Bruno, M. P. Lightfoot, and S. C. Ward. 2016. "The Cambridge Structural Database." *Acta Crystallographica Section B: Structural Science, Crystal Engineering and Materials* 72: 171–179.
- Hirshfeld, F. L. 1977. "Bonded-Atom Fragments for Describing Molecular Charge Densities." *Theoretica Chemica Acta* 44: 129–138.
- Kabekkodu, S., A. Dosen, and T. N. Blanton. 2024. "PDF-5+: A Comprehensive Powder Diffraction file™ for Materials Characterization." *Powder Diffraction* 39: 47–59.
- Kaduk, J. A., C. E. Crowder, K. Zhong, T. G. Fawcett, and M. R. Suchomel. 2014. "Crystal Structure of Atomoxetine Hydrochloride (Strattera), C₁₇H₂₂NOCl." *Powder Diffraction* 29: 269–273.
- Kempster, C. J. E. and H. Lipson. 1972. "A Rapid Method for Assessing the Number of Molecules in the Unit Cell of an Organic Crystal." *Acta Crystallographica Section B: Structural Crystallography and Crystal Chemistry* 28: 3674–3674.
- Kim S., J. Chen, T. Cheng, A. Gindulyte, J. He, S. He, Q. Li, B. A. Shoemaker, P. A. Thiessen, B. Yu, L. Zaslavsky, J. Zhang, and E. E. Bolton. 2023. "PubChem 2023 update." *Nucleic Acids Research* 51(D1):D1373–D1380; <https://doi.org/10.1093/nar/gkac956>.
- Kresse, G., and J. Furthmüller. 1996. "Efficiency of Ab-Initio Total Energy Calculations for Metals and Semiconductors Using a Plane-Wave Basis Set." *Computational Materials Science* 6: 15–50.
- Leontowich, A. F. G., A. Gomez, B. Diaz Moreno, D. Muir, D. Spasyuk, G. King, J. W. Reid, C.-Y. Kim, and S. Kycia. 2021. "The Lower Energy Diffraction and Scattering side-Bounce Beamline for Materials Science at the Canadian Light Source." *Journal of Synchrotron Radiation* 28: 1–9; <https://doi.org/10.1107/S1600577521002496>.
- Macrae, C. F., I. Sovago, S. J. Cottrell, P. T. A. Galek, P. McCabe, E. Pidcock, M. Platings, G. P. Shields, J. S. Stevens, M. Towler, and P. A. Wood. 2020. "Mercury 4.0: From Visualization to Design and Prediction." *Journal of Applied Crystallography* 53: 226–235.
- Materials Design. 2024. *MedeA 3.7.2*. San Diego, CA: Materials Design Inc.
- MDI. 2024. *JADE Pro version 9.0*. Livermore, CA: Materials Data.
- Motherwell, W. D. S., G. P. Shields, and F. H. Allen. 2000. "Graph-Set and Packing Analysis of Hydrogen-Bonded Networks In Polyamide Structures In the Cambridge Structural Database." *Acta Crystallographica B* 56: 857–871.
- Peintinger, M. F., D. Vilela Oliveira, and T. Bredow. 2013. "Consistent Gaussian Basis Sets of Triple-Zeta Valence with Polarization quality for Solid-State Calculations." *Journal of Computational Chemistry* 34: 451–459.
- Rammohan, A. and J. A. Kaduk. 2018. "Crystal Structures of Alkali Metal (Group 1) Citrate Salts." *Acta Crystallographica Section B: Crystal Engineering and Materials* 74: 239–252.
- Spackman, P. R., M. J. Turner, J. J. McKinnon, S. K. Wolff, D. J. Grimwood, D. Jayatilaka, and M. A. Spackman. 2021. "CrystalExplorer: A Program for Hirshfeld Surface Analysis, Visualization and Quantitative Analysis of Molecular Crystals." *Journal of Applied Crystallography* 54: 1006–1011; <https://doi.org/10.1107/S1600576721002910>.
- Stephens, P. W. 1999. "Phenomenological Model of Anisotropic Peak Broadening in Powder Diffraction." *Journal of Applied Crystallography* 32: 281–289.
- Sykes, R. A., P. McCabe, F. H. Allen, G. M. Battle, I. J. Bruno, and P. A. Wood. 2011. "New Software for Statistical Analysis of Cambridge Structural Database Data." *Journal of Applied Crystallography* 44: 882–886.
- Toby, B. H., and R. B. Von Dreele. 2013. "GSAS II: The Genesis of a Modern Open Source All Purpose Crystallography Software Package." *Journal of Applied Crystallography* 46: 544–549.
- van de Streek, J., and M. A. Neumann. 2014. "Validation of Molecular Crystal Structures from Powder Diffraction Data with Dispersion-Corrected Density Functional Theory (DFT-D)." *Acta Crystallographica Section B: Structural Science, Crystal Engineering and Materials* 70: 1020–1032.
- Wavefunction, Inc. 2023. *Spartan '24. V. 1.0.0*. Irvine CA: Wavefunction Inc.